

Formation of p-n junction in polymer electrolyte-top gated bilayer graphene transistor

Biswanath Chakraborty, Anindya Das and A. K. Sood*

Department of Physics, Indian Institute of Science , Bangalore - 560012, India

Abstract

We show simultaneous p and n type carrier injection in bilayer graphene channel by varying the longitudinal bias across the channel and the top gate voltage. The top gate is applied electrochemically using solid polymer electrolyte and the gate capacitance is measured to be $1.5 \mu F/cm^2$, a value about 125 times higher than the conventional SiO_2 back gate capacitance. Unlike the single layer graphene, the drain-source current does not saturate on varying the drain-source bias voltage. The energy gap opened between the valence and conduction bands using top and back gate geometry is estimated.

PACS numbers:

*Electronic address: asood@physics.iisc.ernet.in

I. INTRODUCTION

In recent years, single and a few layer graphene are at the center stage of intense research to unravel physical properties of these new forms of carbon, with an eye on device applications. Ultra high mobilities and observation of ballistic transport make graphene based devices a potential alternative for silicon based devices [1, 2, 3, 4]. The zero energy gap between the valence and conduction band in the energy spectrum of single layer graphene (SLG) makes it difficult to achieve a high on-off ratio in field effect transistor (FET). On the other hand, bilayer graphene (BLG) devices hold greater promise in terms of better device performance with larger on-off ratio. This is feasible because of the band gap opening due to the breaking of inversion symmetry of the two layers in an otherwise gapless energy band structure. Moreover, this gap between the conduction and valence band can be tuned by means of external gate electric field, as demonstrated both theoretically [5, 6, 7, 8, 9] and experimentally [10, 11, 12, 13]. In particular, Zhang et al. [13] have reported a direct observation of the band gap in the bilayer by infrared absorption. They have used dual gate bilayer FET where 80 nm Al_2O_3 film was used as the top gate and 285 nm SiO_2 as the back gate.

Misewich et al.[14] have shown that it is possible to get polarized infrared optical emission from a carbon nanotube FET by creating an effective forward biased p-n junction along the nanotube channel. This was achieved by applying the gate-drain voltage V_{GD} , comparable to the drain-source voltage V_{DS} , and maximum emission was obtained when $V_{GD} = \frac{V_{DS}}{2}$. Electrical measurements showed that the optical emissions results from the radiative recombination of electrons and holes near the junction. Similar experiments carried out by Meric et. al. [15] on single layer graphene (SLG) device have reported formation of p-n junction along the graphene channel. However, owing to the absence of the band gap in SLG, the recombination of electrons and holes at/near the junction does not yield any radiation. In comparison, bilayer graphene (BLG) device can serve as a prospective candidate in this regard since a band gap can be opened and controlled simultaneously by application of external electric field perpendicular to the layers. Thus, by creating a p-n junction along the bilayer channel by proper biasing of the device, we may be able to fabricate novel source

of terahertz radiation [16, 17] based on the recombination of carriers.

In this paper we show that the BLG device can change from unipolar state to ambipolar state by varying the drain-source bias along the bilayer channel at different top gate voltages (V_T). This has been possible because of very high gate capacitance of the top gate. We also report a quantitative analysis of the band gap opening in the bilayer graphene energy spectrum. In order to control the gap and the position of the Fermi level independently, we have used the top and back gate device geometry. Solid polymer electrolyte and 300nm thick SiO_2 were used as top gate and back gate materials, respectively. This top gate arrangement allows us to shift the Fermi energy significantly by applying a very small top gate voltage (~ 1 V) because of its higher gate capacitance due to nanometer thick Debye layer[18]. In addition, our top gate geometry is a very simple way as compared to depositing high κ dielectric electric materials like HfO_2 and Al_2O_3 , using atomic layer deposition technique. We determine the top gate capacitance accurately by an application of top and back gates on a bilayer graphene device. It is shown that our device has very high gate capacitance $\sim 1.5\mu\text{F}/\text{cm}^2$, which is nearly 125 times larger compared to the gate capacitance of 300 nm SiO_2 ($12\text{ nF}/\text{cm}^2$).

II. EXPERIMENTS AND RESULTS

The device consists of bilayer graphene flake prepared from micromechanical cleavage of highly oriented pyrolytic graphite (HOPG) and deposited on Si/ SiO_2 substrate with the oxide thickness (t) of 300 nm. The electrical contacts on the bilayer device were made by e-beam lithography, followed by thermal evaporation of 30 nm of gold and subsequent liftoff in acetone. The source drain separation (L) is $\sim 500\text{nm}$ and the width (W) is $\sim 5\mu\text{m}$. All the measurements were done at room temperature using two probe contacts. The drain-source and both the top and back gate biases were given from Keithley 2400 source meters. The top gate material solid polymer electrolyte consists of LiClO_4 and polyethylene oxide (PEO) in the ratio 0.12:1 [18, 19, 20]. The top gate voltage (V_T) was applied by inserting a platinum electrode within the polymer layer. Figure 1(a) shows a schematic of the experimental set up. Raman spectroscopy using 514.5 nm excitation laser was used to identify the bilayer graphene (BLG) [21]. Raman spectrum of the bilayer graphene with the 2D mode resolved into four peaks is shown in figure 1(b). Figure 1(c) shows the ambipolar nature of I_{DS} as a

function of V_T for $V_{DS} = 10$ mV and the back gate voltage $V_B = 0$ V. The Dirac point is at $V_T^D = -0.5$ V, implying that our starting sample was electron doped. Mobility (μ), the minimum carrier concentration (δn) and the total contact resistance (R_C) are extracted by fitting the data to an equation based on diffusive transport model,

$$\begin{aligned} R &= R_C + R_G \\ &= R_C + \frac{L}{W} \frac{1}{e\mu\sqrt{(\delta n)^2 + (n_T)^2}} \end{aligned} \quad (1)$$

where R_G is the resistance of the bilayer graphene, n_T is the carrier density induced by the top gate and μ , δn and R_C are the fitting parameters and the contact resistance (R_C) is mainly at the source and drain contacts of the graphene and δn , arises mainly from charge puddles which are created due to charge impurities (n_{imp}) [22, 23] lying between dielectric and the bilayer sample. In order to determine n_T , we estimate the value of the top gate capacitance C_T as follows.

A. Determination of polymer gate capacitance C_T

Figure 2 shows the resistance of the channel as a function of V_B for a fixed V_T . For a given gate voltage V_G ,

$$V_G = \frac{E_F}{e} + \phi = \frac{E_F}{e} + \frac{ne}{C_G} \quad (2)$$

where $\frac{E_F}{e}$ is determined by the quantum capacitance of the bilayer and potential ϕ from the geometrical capacitance of the gate [18, 19]. In equation (2), for top gate $C_G = C_T$, $V_G = V_T$, $n = n_T$; similarly for back gate $C_G = C_B$, $V_G = V_B$, $n = n_B$. The gate-induced carrier density in a bilayer graphene is given by [19, 24]

$$n = \alpha[\gamma_1 E_F + E_F^2], \quad E_F < \gamma_1 \quad (3)$$

where γ_1 is the inter-layer hopping energy (~ 390 meV), $\alpha = \frac{1}{\pi(\hbar v_F)^2}$ and v_F is the Fermi velocity $= 10^6$ m/sec [3]. Therefore, for a given V_T , the induced carrier density in the bilayer sample is

$$n_T = \alpha(\gamma_1 A + A^2) = f(C_T, V_T) \quad (4)$$

where

$$A = -\frac{1}{2}\left(\gamma_1 + \frac{C_T}{\alpha e^2}\right) + \frac{1}{2}\sqrt{\left(\gamma_1 + \frac{C_T}{\alpha e^2}\right)^2 + \frac{4C_T V_T}{\alpha e}} \quad (5)$$

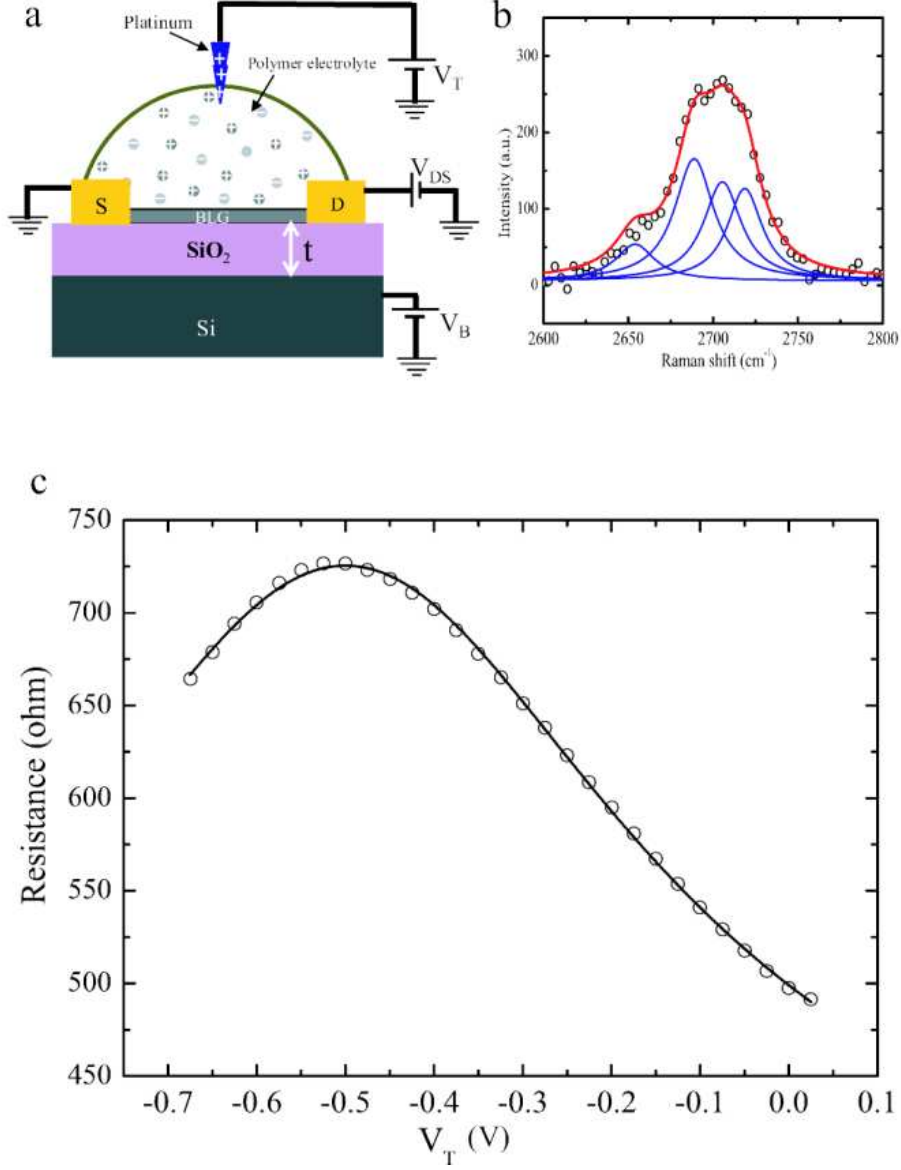


FIG. 1: (Color online) (a) Schematic of the experimental set up showing the top and back gate arrangement. (b) Raman spectrum of the bilayer graphene showing its characteristic 2D modes. (c) Resistance vs top gate voltage (V_T). Open circles are experimental data and the solid line is fit to equation (1).

Similar expressions hold good for the back gate geometry and when resistance is maximum (R_m) at a back gate voltage V_B^{max} , $|n_T| = |n_B|$ to make the Fermi energy shift zero. Therefore, for a given V_T

$$f(C_T, V_T) = f(C_B, V_B^{max}) \quad (6)$$

where C_T is the only unknown parameter. Using the known $C_B = 12nF/cm^2$ and V_B^{max} for different V_T , the average value of C_T is found to be $\sim 1.5\mu F/cm^2$. Note that, in this estimation the quantum capacitance is not assumed to be a constant as was done by Meric et. al.[15]. Knowing C_T , n_T is thus determined as a function of V_T from equation (4) and (5). The experimental curve of figure 1c is then fitted to equation (1) giving, $\mu = 730$ $cm^2/V.sec$, $\delta n = 1.5 \times 10^{12}/cm^2$ and $R_C = 150 \Omega$.

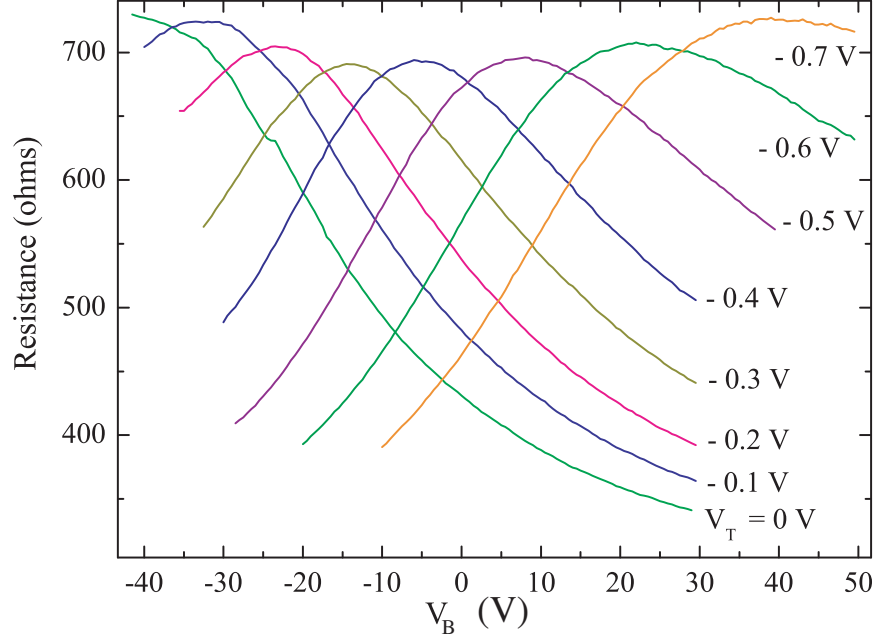


FIG. 2: (Color online) Resistance vs back gate voltage (V_B) for a fixed value of V_T .

B. Formation of p-n junction along the bilayer channel

We now discuss the characteristics of drain-source current (I_{DS}) as a function of drain-source bias (V_{DS}). Figure 3(a) and b shows I_{DS} vs V_{DS} for different top gate voltages. The main noticeable feature is a clear non-linear dependence of I_{DS} on V_{DS} , and a significant effect of the gate voltage on the shape of the $I_{DS} - V_{DS}$ curves.

To understand the non-linear $I_{DS} - V_{DS}$ curve, we look at the schematic in figure 4(a). For $V_{DS} \ll V_T$, the bilayer channel will be electron doped for $(V_T - V_T^D) > 0$ and hole doped for $(V_T - V_T^D) < 0$ and the doping ($n(x)$) will be homogeneous along the channel length. However, this is not the case when V_{DS} is comparable to V_T . In this case the voltage difference between the gate and the bilayer channel varies from $(V_T - V_T^D)$ at the source to

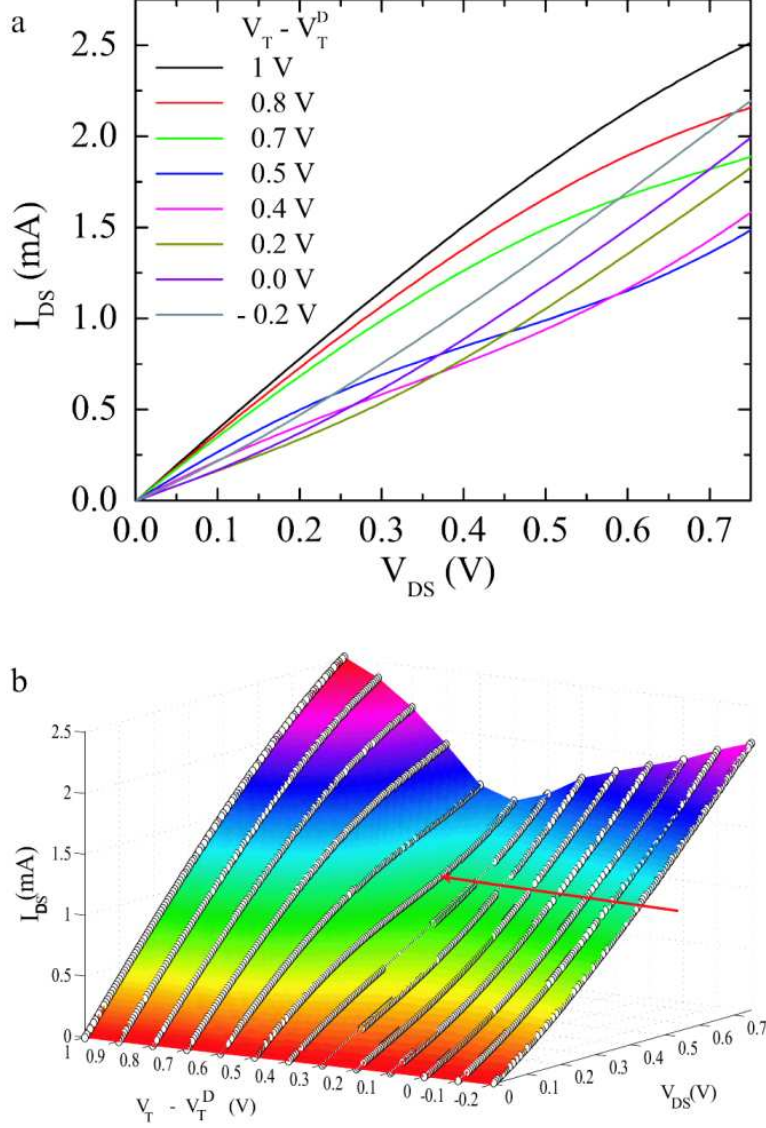


FIG. 3: (Color online) (a) I_{DS} versus (V_{DS}) as a function of $V_T - V_T^D$ for $V_B = 0V$. (b) 3D plot showing the variation of I_{DS} as function of both T and V_{DS} . The point of inflection is shown by an arrow.

$V_{DS} - (V_T - V_T^D)$ at the drain electrode. Therefore, by varying drain-source voltage (V_{DS}) at fixed V_T , the doping concentration $n(x)$ changes from n type to p type along the channel length. In figure 4(a), we have shown the carrier distribution $n(x)$, along the bilayer channel for three different cases of drain-source voltage (V_{DS}) at $(V_T - V_T^D) = 0.5$ V.

Case 1: $V_{DS} < (V_T - V_T^D)$, and therefore the carriers $n(x)$ will be electrons in the bilayer channel with $n(x = 0) > n(x = L)$. In this region, I_{DS} increases sub linearly with V_{DS}

because the average carrier concentration $[< n(x) > = \frac{1}{L} \int_0^L n(x) dx]$ decreases with V_{DS} .

Case 2: $V_{DS} = (V_T - V_T^D)$, $n(x)$ will be zero at $x = L$ and therefore, the conduction channel gets pinched off near the drain end making the region devoid of charge carriers. At this point the slope of the I_{DS} vs V_{DS} curve undergo a change (figure 4(b)).

Case 3: $V_{DS} > (V_T - V_T^D)$, the point in the channel where the pinch off occurs, moves deeper into the channel drifting towards the source electrode. As $V_{DS} > (V_T - V_T^D)$, the gate is negatively biased with respect to drain near the drain region. As a result carrier concentration $n(x)$ will be holes near the drain region, as shown in the lower most panel of figure 4(a). When V_{DS} is increased beyond pinch off, the current increases due to enhanced p channel conduction.

Thus the bilayer channel is now viewed as comprising of distinct electron and hole regions, with the electron doped region shrinking as the applied drain-source bias is increased. The potential drop across the electron channel remains fixed at $V_T - V_T^D$ while the drop across the hole region (from drain end to pinch off) increases as $V_{DS} - (V_T - V_T^D)$, with the applied drain-source bias. As the device is operated beyond the pinch off, the dominant current carrier changes from electron to holes and the current increases as a function of V_{DS} . It appears as if a forward biased p-n junction is formed at the pinch off region, with p-region towards the drain end and n-region towards the source region.

A noticeable feature is the absence of current saturation in all the I_{DS} vs V_{DS} curves as compared to the monolayer case reported recently [15]. In order to address if the small length of the channel in our experiment ($\sim 500\text{nm}$) is responsible for non-saturation of current [15, 25], we carried out experiments on a device of drain-source separation $\sim 2.5\mu\text{m}$ and width $\sim 1.5\mu\text{m}$. This also did not show any signature of current saturation.

In order to analyze the I_{DS} - V_{DS} curves, we model the drain current as

$$I_{DS} = \frac{W}{L} \int_0^L e v_D(x) \sqrt{(\delta n)^2 + (n_T(x))^2} dx \quad (7)$$

where $v_D(x)$ is drift velocity. The drift velocity can be written as

$$v_D(x) = \mu E(x) = \mu \frac{dV(x)}{dx} \quad (8)$$

where E is the longitudinal electric field due to drain-source bias, $V(x)$ is the potential drop

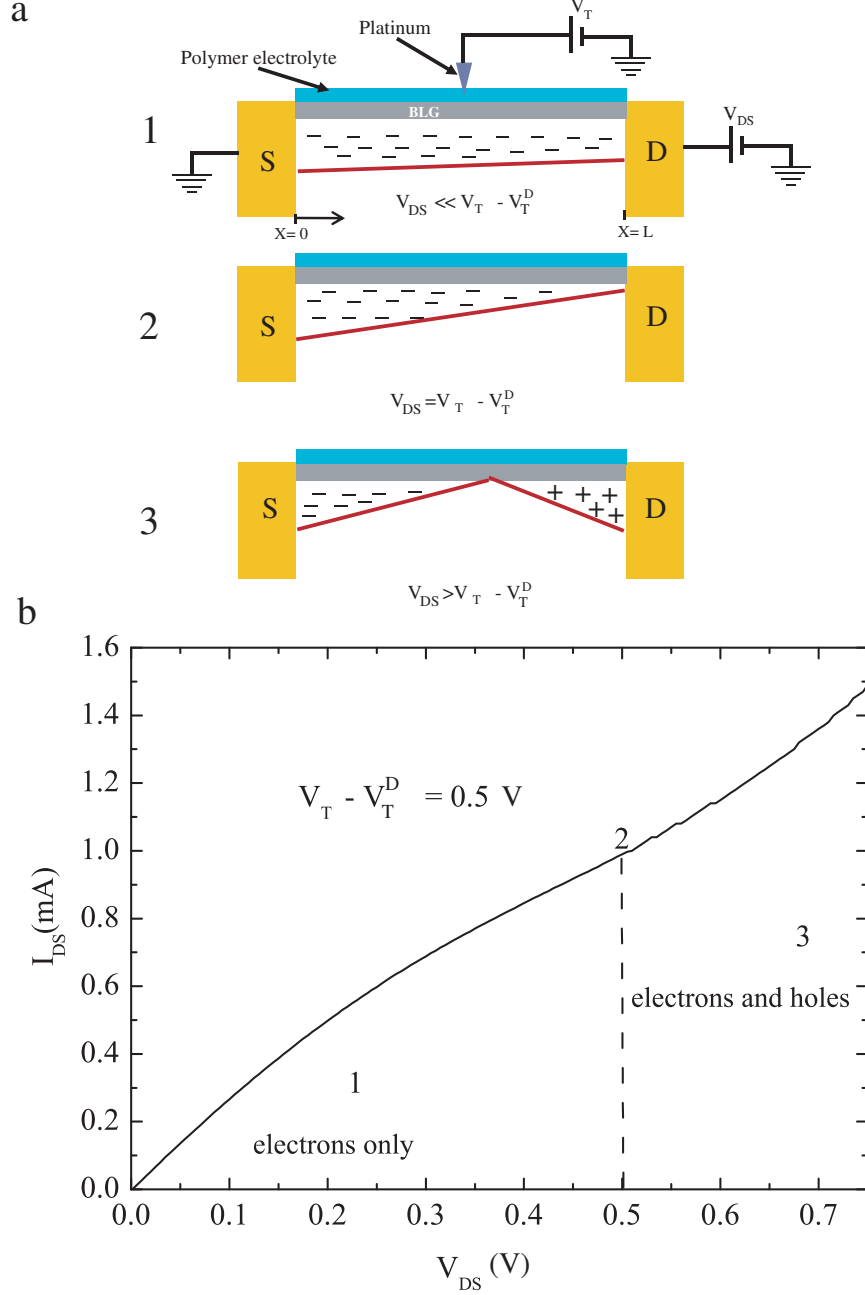


FIG. 4: (Color online) (a) Schematic of the spatial profile of the carrier concentration ($n(x)$) along the channel for a particular top gate voltage. Three cases are shown: Case 1: ($V_{DS} \ll V_T - V_T^D$) when the carriers are only electron; Case 2: $V_{DS} = V_T - V_T^D$ when the pinch off starts appearing near the drain end and case 3: $V_{DS} > V_T - V_T^D$ where the minimum carrier density point (pinch off) shifts towards the source end. (b) I_{DS} - V_{DS} curve for $V_T - V_T^D = 0.5V$ pointing out the regions mentioned in Fig.4a. An inflection point appears at $V_{DS} = V_T - V_T^D = 0.5 V$ implying pinch off at drain end.

at point x in the channel and μ is the mobility. Therefore,

$$I_{DS} = \frac{W}{L} e \mu \int_{I_{DS} \frac{R_C}{2}}^{V_{DS} - I_{DS} \frac{R_C}{2}} \sqrt{(\delta n)^2 + (n_T)^2} dV \quad (9)$$

where the upper and lower limits signifies the voltage drop at the drain and source ends, respectively. The drop due to the contact resistance at both the ends has been assumed to be equal. Using the extracted values of the mobility (μ), the contact resistance (R_C), δn and n_T , equation (9) is solved numerically. Figure 5 shows experimental data (open circles) for three top gate voltages along with the theoretical curves (solid lines). It can be noted that agreement between the experiment and the calculation is quite good.

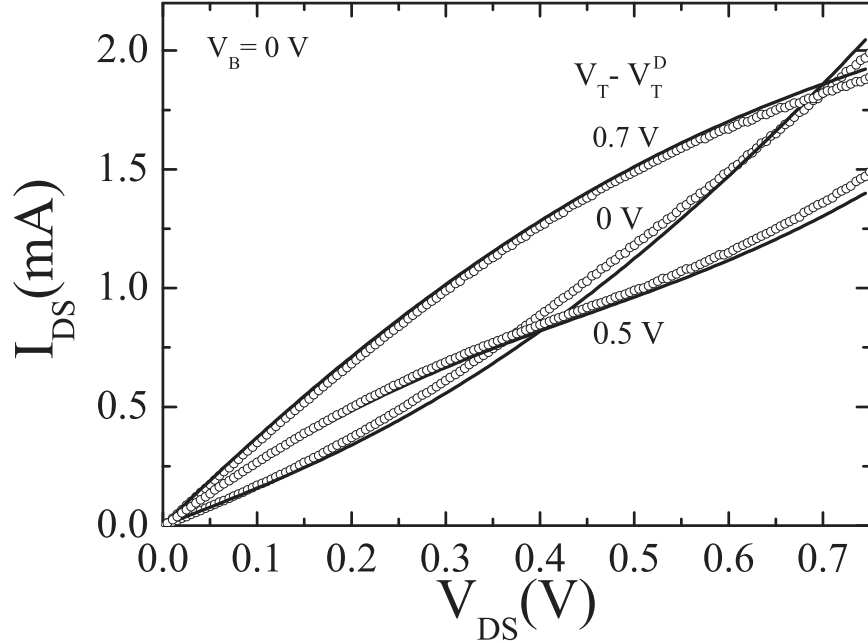


FIG. 5: (Color online) Comparison between experiment(open circles) and theory(solid lines) is done for three gate voltages.

C. Opening of energy gap in bilayer graphene and its estimation

Coming back to figure 2, it shows resistance as a function of the back gate voltage for a fixed top gate voltage. For $V_T = 0$ V, the maximum value of resistance (R_m) at a negative back gate voltage ($V_B = V_B^* \sim -40$ V) clearly establishes that the bilayer graphene channel is intrinsically n-doped. Figure 2 shows that the value of R_m is minimum at $V_T = -0.4$ V and

increases almost symmetrically on changing V_T . It can also be seen, that for a particular top gate voltage, the drain-source current is not symmetric for electron and hole doping.

The change in the maximum value of resistance (R_m) at different top gate voltages arises due to the opening of an energy gap between the conduction and valence bands of the bilayer graphene [5, 10, 11, 12, 13]. It has been shown both theoretically [6, 7, 8] and experimentally [5, 10, 11, 12, 13] that a difference between the on-site energy in the layers leads to an opening of the gap between conduction and valence band which touch each other at the zone edge K point of brillouin zone [8]. This on-site energy difference can be controlled externally by the application of electric field, perpendicular to the layers, which implies a potential energy difference ΔV and hence a gap Δ_g . Experimentally such fields in-between two carbon layers were created either by application of top and bottom gates simultaneously [11, 12, 13] or by chemical doping of a back gated device [5, 10]. In the presence of an electric field in between the layers, the Hamiltonian for the bilayer graphene near the K point can be written as

$$\mathbf{H} = \begin{pmatrix} -\Delta V/2 & \gamma \mathbf{k} & 0 & 0 \\ \gamma \mathbf{k} & -\Delta V/2 & \gamma_1 & 0 \\ 0 & \gamma_1 & \Delta V/2 & \gamma \mathbf{k} \\ 0 & 0 & \gamma \mathbf{k} & \Delta V/2 \end{pmatrix} \quad (10)$$

with, $\gamma = \frac{\sqrt{3}}{2}\gamma_0 a$ where γ_0 and γ_1 are the inplane and interlayer nearest neighbor hopping energies respectively. The eigen-values of the above Hamiltonian for the lower subbands of the bilayer graphene can be written as :

$$\epsilon_{\pm}(k) = \pm \sqrt{\left(\frac{(\Delta V)^2}{4} + \frac{\gamma_1^2}{2} + \gamma^2 k^2\right) - \sqrt{\frac{\gamma_1^4}{4} + \gamma^2 k^2 (\gamma_1^2 + (\Delta V)^2)}} \quad (11)$$

where \pm correspond to conduction and valence bands, respectively. Figure 6(a) shows the band structure of bilayer graphene having a band gap (Δ_g). The relation between the band gap and potential energy difference (ΔV) is given by [8]

$$\Delta_g = \sqrt{\gamma_1^2 (\Delta V)^2 / (\gamma_1^2 + (\Delta V)^2)} \quad (12)$$

which shows that there will be no band gap if $\Delta V = 0$.

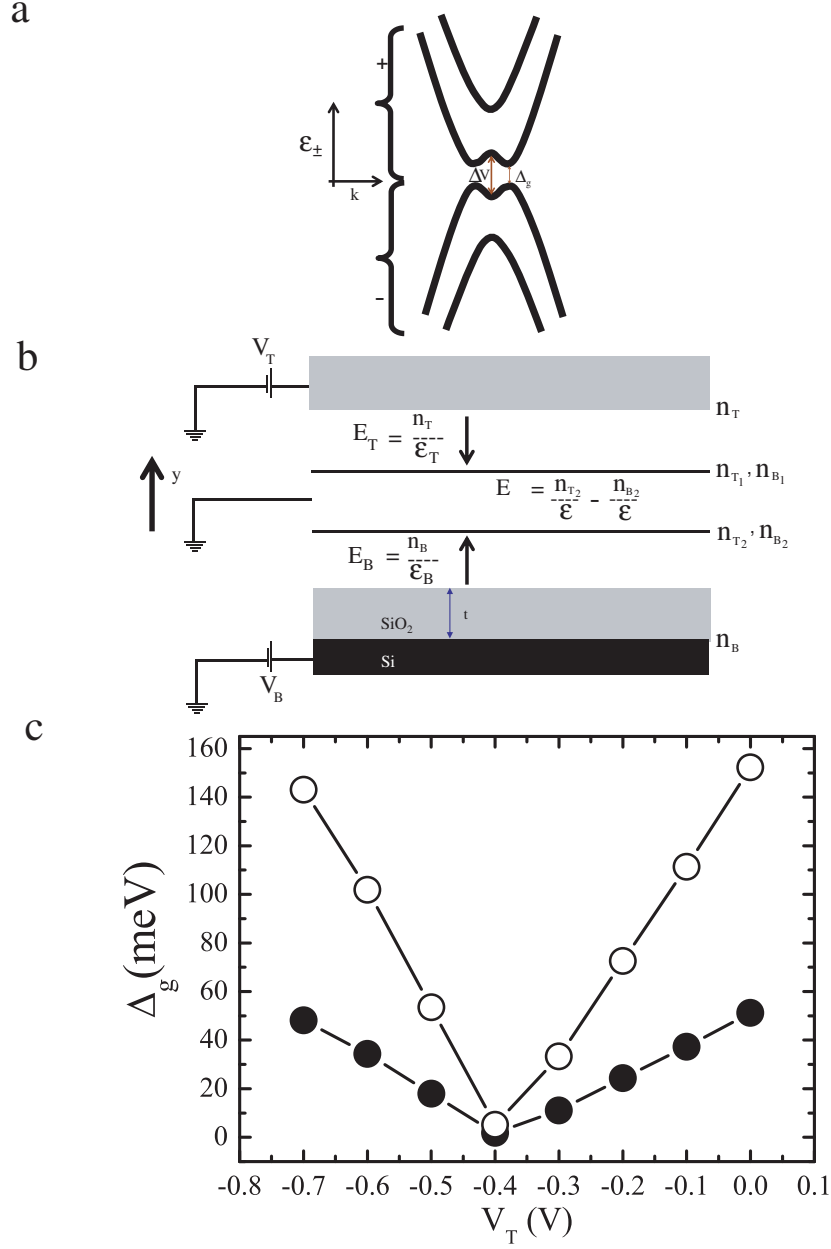


FIG. 6: (Color online) (a) Band structure of the biased bilayer graphene. (b) Schematic of the electric fields between the carbon layers. The arrows show the direction of the electric fields. (c) Energy gap Δ_g as a function V_T . The open (filled) circles show the values of the gap without (with) screening.

Figure 6(b) shows the induced carrier density in each carbon layer along with the electric field in between them in the presence of top and back gates. The total induced carrier density in bilayer, due to V_T is: $n_T e = -C_T V_T$ and similarly, for V_B , $n_B e = -C_B V_B$. Therefore,

total induced carrier density in bilayer graphene due to top and back gates is:

$$ne = n_T e + n_B e = -[C_T V_T + C_B V_B] \quad (13)$$

where, for simplicity, we have neglected the quantum capacitance. Considering the screened electric field, the induced carrier density due to top gate is n_{T_1} and n_{T_2} where subscripts 1 and 2 refer to top and bottom layers, respectively, as shown in figure 6(b). For a screening length of λ , we can write for top gate $n_{T_2} = n_{T_1} e^{-d/\lambda}$ where d is the separation between the two layers (3.41Å). Thus, for the top gate $n_T = n_{T_1} + n_{T_2}$ and $n_{T_2} = \frac{n_T}{1+e^{d/\lambda}}$. Similar expression holds good for the back gate. Thus, in presence of back and top gates the resultant electric field inside the bilayer would be $\vec{E} = \vec{E}_T + \vec{E}_B$, where

$$\begin{aligned} E_T &= \frac{n_T e}{2\epsilon} - \frac{n_{T_1} e}{2\epsilon} + \frac{n_{T_2} e}{2\epsilon} \\ &= \frac{n_{T_2} e}{\epsilon} = \frac{n_T e}{\epsilon(1 + e^{d/\lambda})} = \frac{C_T V_T}{\epsilon(1 + e^{d/\lambda})} \end{aligned} \quad (14)$$

where $\epsilon \sim 2.5$ is the dielectric constant of the bilayer graphene [8].

The same analysis holds good for E_B as well. Therefore, the net electric field between two carbon layers is,

$$\vec{E} = -\hat{y} \left[\frac{C_T V_T}{\epsilon(1 + e^{d/\lambda})} - \frac{C_B V_B}{\epsilon(1 + e^{d/\lambda})} \right] \quad (15)$$

It should be noted that for $\lambda = \infty$ the equation (15) reduces to

$$\vec{E} = -\hat{y} \left[\frac{C_T V_T}{2\epsilon} - \frac{C_B V_B}{2\epsilon} \right] \quad (16)$$

i.e. the field without screening which corresponds to two layers having equal carrier density.

It can be seen from equation (13) and (15) that minimal value of the resistance maximum should appear when $V_B = 0$ V and $V_T = 0$ V, since this would imply that Fermi energy $E_F = 0$ (since $n = 0$) and band gap $\Delta g = 0$ (since $E = 0$). As mentioned earlier, in our experiment minimum value of R_m appears at $V_T = -0.4$ V (figure 2) because of unintentional electron doping. To consider the effect of electric field inside the bilayer due to this unintentional electron doping, we place a positive charge sheet of carrier density n_0 above the top carbon

layer, given by $n_0 = C_B V_B^*$ obtained from the back gate sweep for $V_T = 0$ V, as shown in figure 2 ($V_B^* \sim -40$ V). Thus the net electric field inside the bilayer is written as

$$\vec{E} = \vec{E}_T + \vec{E}_B + \vec{E}_0 = -\hat{y} \frac{1}{\epsilon(1 + e^{d/\lambda})} [C_T V_T - C_B V_B + C_B V_B^*] \quad (17)$$

where \vec{E}_0 is the field due to n_0 . The potential energy difference between the two layers is $\Delta V = e(E \times d)$, and the value of the gap is estimated from equation (12). Taking back gate capacitance $C_B = 12 \text{ nF/cm}^2$ and top gate capacitance $C_T \sim 1.5 \mu\text{F/cm}^2$, figure 6c shows the plot of the value of the band gap, with screening $\lambda = 5 \text{ \AA}$ [3] and without screening $\lambda = \infty$, as a function of V_T (where band gap values are evaluated at R_m for each of the back gate characteristic at fixed V_T (figure 2)). It can be seen from figure 6c, that Δ_g is minimum at $V_T = -0.4$ V. This trend follows from the trend of R_m (see figure 2). We notice that, had the arrangement of n_0 been placed below the bottom layer, then the field components associated with it would have changed their direction and the calculated energy gap would not have followed the trend of R_m . Thus, our assumption that the arrangement of unintentional carrier density n_0 lies above the top layer has indeed been justified

III. CONCLUSIONS

In conclusion, the bilayer channel transforms from n type to p type conduction channel as we vary the drain-source voltage. This variation results in nonlinear dependence of I_{DS} on V_{DS} as a function of V_T which has been quantitatively explained. Contrary to the recently reported monolayer case, we did not observe any signature of current saturation for I_{DS} . In the presence of a gap in bilayer energy spectrum, the formation of p-n junction creates new possibility for the bilayer device as a source of terahertz radiation [16, 17], similar to infrared emission from the carbon nanotubes [14]. The radiation from recombination between electrons and holes at the junction may acts as terahertz source depending on the magnitude of the gap that can be opened. The opening of a gap in the bilayer spectrum was studied, where the gap was controlled using a top and back gate geometry. However the band gap opening is limited by the restriction on the back gate voltage, since the breakdown field for the SiO_2 is 1 V/nm (up to 300 V in our case). The capacitance of the polymer electrolyte was determined accurately. Thus solid polymer electrolyte gating of graphene devices may open up new avenues for graphene based electronics, particularly where higher

carrier concentration is required.

Acknowledgments

AKS thanks Department of Science and Technology for financial assistance through the DST Nanoscience Initiative Project.

References

-
- [1] Novoselov K S, Geim A K, Morozov S V, Jiang D, Zhang Y, Dubonos S V, Grigorieva I V and Firozov A A 2004 *Science* **306** 666-669
 - [2] Novoselov K S, Geim A K, Morozov S V, Jiang D, Katnelson M I, Grigorieva I V, Dubonos S V, and Firozov A A 2005 *Nature* **438** 197-200
 - [3] Geim A K, and Novoselov K S 2007 *Nature Materials* **6** 183-191
 - [4] Bolotin K I, Sikes K J, Stormer H L and Kim P 2008 *Phys. Rev. Lett.* **101** 096802
 - [5] Castro E V, Novoselov K S, Morozov S V, Peres N M R, Lopes dos Santos J M B, Nilsson J, Guinea F, Geim A K and Castro Neto A H 2007 *Phys. Rev. Lett.* **99** 216802
 - [6] McCann E, 2006 *Phys. Rev. B* **74** 161403(R)
 - [7] McCann E and Falko V I 2006 *Phys. Rev. Lett.* **96** 086805
 - [8] Castro E V, Novoselov K S, Morozov S V, Nilsson J, Guinea F, Geim A K and author Castro Neto A H *e-print arXiv:cond-mat/0807.3348v1*
 - [9] Gava P, Lazzeri M, Saitta A M and Mauri F *e-print arXiv:cond-mat/0902.4615v1*
 - [10] Ohta T, Bostwick A, Seyller T, Horn K and Rotenberg E 2006 *Science* **313** 951-954
 - [11] Ostinga J B, Heersche H B, Liu X and Morpugo A F 2008 *Nature Materials* **7** 151-157
 - [12] Pal A N and Ghosh A 2009 *Phys. Rev. Lett.* **102** 126805
 - [13] Zhang Y, Tang T, Girit C, Hao Z, Martin M C, Zettl A, Crommie M F, Shen Y R, Wang F 2009 *Nature* **459** 820-823
 - [14] Misewich J A, Martel R, Avouris Ph, Tsang J. C, Heinze S and J. Tersoff 2003 *Science* **300** 783-786

- [15] Meric I, Han M Y, Young A F, Ozyilmaz B, Kim P and Shepard K L 2008 *Nature Nanotechnology* **3** 654-659
- [16] Berman O L, Gumbs G and Lozovik Y E 2008 *Phys. Rev. B* **78** 085401
- [17] Aleshkin V Y, Dubinov A A and Ryzhii V 2009 *JETP Letters* **89** 63-67
- [18] Das A, Pisana S, Chakraborty B, Piscanec S, Saha S K, Waghmare U V, Novoselov K S, Krishnamurthy H R, Geim A K, Ferrari A C and Sood A K 2008 *Nature Nanotechnology* **3** 210-215
- [19] Das A, Chakraborty B, Pisana S, Piscanec S, Sood A K and Ferrari A C 2009 *Phys. Rev. B* **79** 155417
- [20] Das A, Sood A K, Govindaraj A, Saitta A M, Lazzeri M, Mauri F and Rao C N R 2007 *Phys. Rev. Lett.* **99** 136803
- [21] Ferrari A C, Meyer J C, Scardaci V, Casiraghi C, Lazzeri M, Mauri F, Piscanec S, Jiang D, Novoselov K S, Roth S and Geim A K 2006 *Phys. Rev. Lett.* **97** 187401
- [22] Adam S, Hwang E H, Galitski V M and Sharma S D 2007 *Proc. Natl. Acad. Sci. USA* **104** 18392-18397
- [23] Martin J, Akerman N, Ulbricht G, Lohmann T, Smet J H, von Klitzing K and Yacoby A 2008 *Nature Physics* **4** 144-148
- [24] Ando T 2007 *J. Phys. Soc. Jpn* **76** 104711
- [25] Radosavljevic M, Heinze S, Tersoff J, and Avouris Ph 2008 *Appl. Phys. Lett.* **83** 2435-2437